Journal of CO_2 Utilization xxx (2015) xxx–xxx

Contents lists available at ScienceDirect

Journal of CO_2 Utilization

journal homepage: www.elsevier.com/locate/jcou

Mechanistic insights into the Cu(I) oxide-catalyzed conversion of CO_2 to fuels and chemicals: A DFT approach

Abhishek Kumar Mishra[a,*], Nora H. de Leeuw[a,b,**]

[a] Department of Chemistry, University College London, 20 Gordon Street, London WC1H 0AJ, UK
[b] School of Chemistry, Cardiff University, Main Building, Park Place, Cardiff CF10 3AT, UK

ARTICLE INFO

Article history:
Received 30 October 2015
Received in revised form 25 January 2016
Accepted 23 February 2016
Available online xxx

Keywords:
Copper oxide
CO_2 hydrogenation
Formic acid
DFT-D
Formate

ABSTRACT

Periodic, self-consistent, density functional theory calculations with corrections via a Hubbard U parameter, and inclusion of dispersive forces (DFT-D2), have been employed to study CO_2 activation and conversion on the Cu_2O (111) surface. CO_2 hydrogenation on the Cu_2O (111) surface was investigated systematically, and the respective microscopic reaction mechanisms were elucidated. We show that, whereas CO_2 dissociation is not energetically allowed on the Cu_2O (111) surface, CO_2 hydrogenation to a formate intermediate is more favourable than the formation of a carboxyl intermediate. Further hydrogenation from formate to formic acid is energetically allowed, where formate combines with strongly adsorbed surface hydrogen to form bidentate formic acid moieties. Formation of both the formate and the formic acid from adsorbed CO_2 and surface hydrogen are exothermic reactions.

1. Introduction

The consistent rise in carbon dioxide (CO_2), mainly due to the consumption of carbon-rich fossil fuels [1,2] has already caused the average carbon dioxide concentration of the Earth's atmosphere to surge past 400 PPM [3,4] and it is expected to reach levels between 700 and 1000 ppm by the end of this century [5]. At present, there is no single technology that can effectively reduce emissions of CO_2 into the atmosphere at the levels required by the Kyoto protocol. While reducing CO_2 emissions is an extensive and long term task, CO_2 is, however, an attractive feedstock of C1 building blocks, allowing production of various value-added products through appropriate catalytic processes [8–11]. Although the capture of CO_2 is an energetically costly procedure and thus far still causes a net increase in the amount of extracted fuel [6,7], the utilization of CO_2 as a source of carbon not only reduces the amount of CO_2 in the atmosphere but also produces fuels and useful chemicals [12–15].

Among the large number of products that could be derived from CO_2, an important feedstock chemical and fuel is formic acid [7,16–18]. Besides its use in a variety of applications, including the textile industry, leather processing, animal feeds and as a food preservative, it is also explored in the controlled generation of hydrogen [19–22]. Owing to a volumetric hydrogen density of 53 g of H_2 per litre, low toxicity and liquid phase under ambient conditions, formic acid is an ideal hydrogen storage material. Recently, efforts have been made to directly synthesize formic acid from carbon dioxide via catalytic hydrogenation, due to its sustainability over other existing routes [18]. Another reason to study the hydrogenation of CO_2 to formic acid (HCO_2H) is the opportunity of direct access to chemicals based on waste products from the use of fossil fuels for energy [12].

Catalysis plays a key role in better carbon management, and catalysts need to be developed for the conversion of the new raw materials that are structurally different from those used today (hydrocarbons) [23,24]. Transition metal-catalysed CO_2 hydrogenation to formic acid is one of the most explored CO_2 fixation reactions [17,25–28], with recent work achieving the electrocatalytic reduction of CO_2 to formic acid in an aqueous environment under moderate reaction conditions over an iron sulfide catalyst [29]. Copper and its alloys are known to produce significant quantities of hydrocarbons from CO_2 [30], whereas copper oxide nanocrystals have found applications in numerous fields [31–41]. Among their different properties, including electrical [33,34] and gas-sensing [41], the catalytic properties [32,40,42] are strongly influenced by different morphological surface structures. For example, direct reduction of CO_2 to methanol at electro-deposited cuprous oxide thin films was observed with 43 $\mu mol\ cm^{-2}\ h^{-1}$ and 38% Faradaic efficiencies [43]. With mixed oxidation states on the copper oxide surface, the Cu(I) species was

* Corresponding author at: Department of Chemistry, University College London, 20 Gordon Street, London WC1H 0AJ, UK
** Corresponding author at: School of Chemistry, Cardiff University, Main Building, Park Place, Cardiff CF10 3AT, UK.
E-mail addresses: abhishek.mishra@ucl.ac.uk (A.K. Mishra), deleeuwn@cardiff.ac.uk (N.H. de Leeuw).

http://dx.doi.org/10.1016/j.jcou.2016.02.008

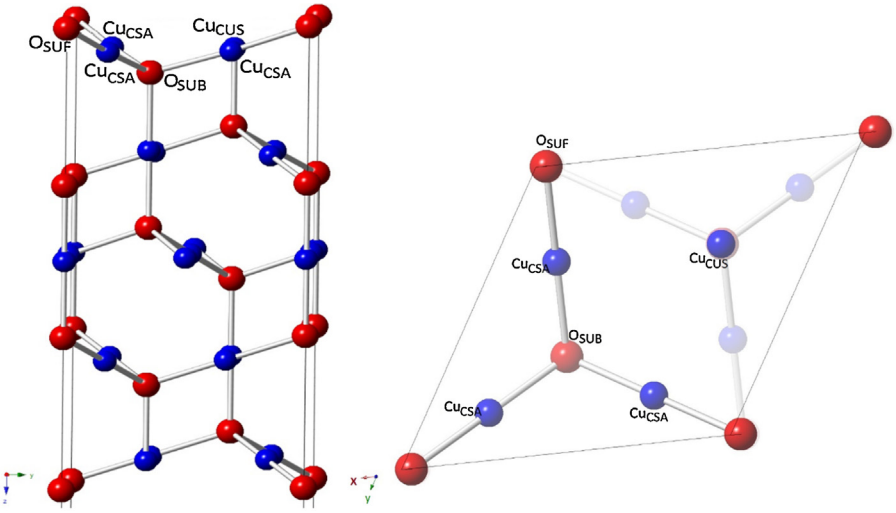

Fig. 1. Schematic presentation of the Cu_2O (111) surface used in the present study: (a) side view and (b) top view. Blue and red colour balls indicate Cu and O atoms respectively in both figures. (For interpretation of the references to colour in this figure legend, the reader is referred to the web version of this article.)

found to play an important role in reducing CO_2 to methanol. However, methanol and formic acid synthesis is a complex multi-step process and a detailed atomic level understanding of the reaction mechanism is necessary to improve catalytic efficiency further. Calculations based on the density functional theory (DFT) are a promising tool to discover new catalysts, e.g. by identifying highly active sites [44–46], and they could help in guiding the catalyst design process and controlled synthesis of the desired products [47]. For example, through DFT calculations, Yang et al. [48] showed that methanol synthesis on Cu surfaces proceeds through a formate intermediate and that the overall reaction is limited by the hydrogenation of both formate and dioxomethylene. While the nature of the active phase of Cu is still in dispute, the low valence of Cu can affect the catalytic efficiency of Cu-based catalysts. Investigation of the electronic and geometrical structures of the active site is a first step towards the rational design of catalysts with desirable activity and selectivity. Because of the complexity of reactions occurring on composite materials, atomic-level understanding is always a challenge in heterogeneous catalysis [49].

In the present work we have studied the hydrogenation of CO_2 on the most stable, (111), surface of Cu_2O. Using DFT calculations, we have gained insight into the elementary steps involved in the methanol formation from CO_2 and hydrogen on the copper oxide-based catalyst. We have systematically studied the reaction mechanism and energetics of CO_2 hydrogenation to formate, carboxyl and formic acid moieties. We first examined the adsorption of CO_2, H_2O and H_2 molecules on the Cu_2O (111) surface individually, followed by the co-adsorption and reaction between CO_2 and atomic hydrogen on the surface. We further present reaction energetics and activation barriers for the formation of formic acid on the surface.

2. Methodology and models

All the calculations were performed in the framework of DFT using the Vienna ab initio simulation package (VASP) with a plane-wave basis set [50–53]. The projector augmented wave method was used to describe the interaction between ions and electrons [54], and the non-local exchange correlation energy was evaluated using the Perdew–Burke–Ernzerhof functional [55,56]. The Hubbard model is used to treat strong correlations within the DFT + U method in the Dudarev formalism [57]. Recently, we have determined a value of U that can efficiently describe both copper I and II oxides [58] and this effective U_{eff} value of 7 eV is selected for the localized 3d electrons of Cu, where $U_{eff} = U - J$, i.e. the difference between the Coulomb U and exchange J parameters, hereafter referred to as U. This value has been shown in our previous work to reproduce to an acceptable accuracy the experimental lattice parameters, magnetic moments, and band gap of copper oxides [58]. We have further used the implementation of the DFT-D2 approach described by Grimme [59] to account for long-range dispersion forces. A plane wave basis set with a cutoff energy of 450 eV and a $5 \times 5 \times 1$ k-point grid generated by the Monkhorst–Pack method [60] were found to give converged results for the surface calculations. The atomic structures were relaxed using the tetrahedron method with Bloch correction as implemented in VASP [61] and the positions of all the atoms in the cell were fully

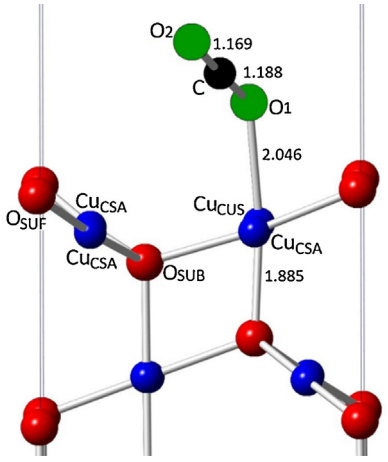

Fig. 2. CO_2 adsorption on the Cu_2O (111) surface showing important bond lengths in Å. Blue and red colour ball indicates Cu and O surface atoms respectively, while O and C atoms of the CO_2 molecule are represented by green and black colour balls respectively. (For interpretation of the references to colour in this figure legend, the reader is referred to the web version of this article.)

Please cite this article in press as: A.K. Mishra, N.H. de Leeuw, Mechanistic insights into the Cu(I) oxide-catalyzed conversion of CO_2 to fuels and chemicals: A DFT approach, J. CO_2 Util. (2016), http://dx.doi.org/10.1016/j.jcou.2016.02.008

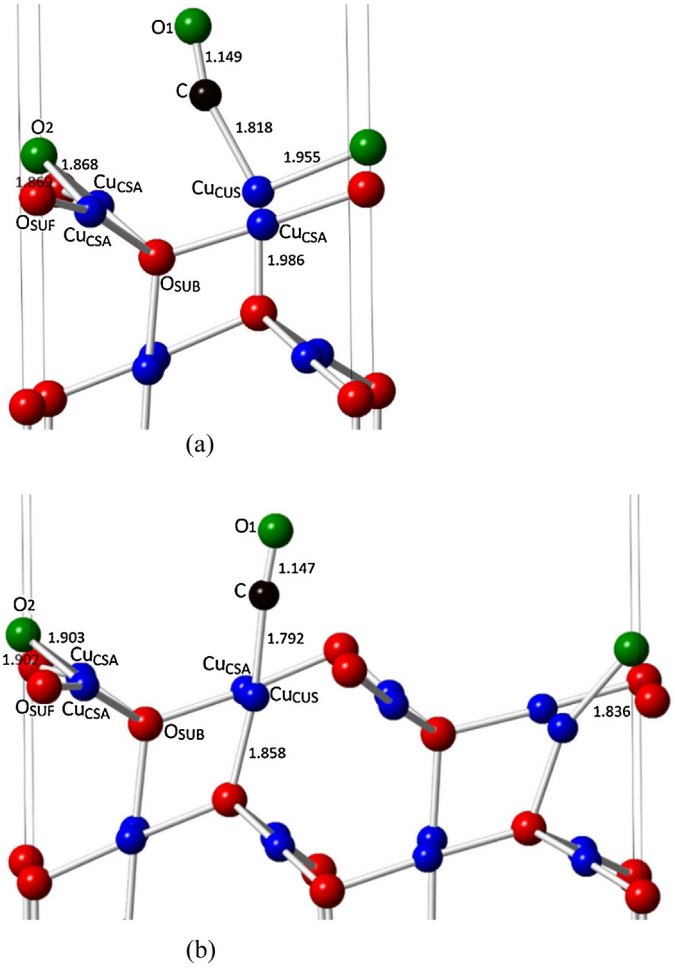

Fig. 3. CO_2 dissociation on the Cu_2O (111) surface in (a) (1 × 1) cell, (b) (2 × 1) supercell, showing important bond lengths in Å. Blue and red colour balls indicate Cu and O surface atoms respectively, while O and C atoms of the CO_2 molecule are represented by green and black colour balls respectively. (For interpretation of the references to colour in this figure legend, the reader is referred to the web version of this article.)

relaxed until the atomic forces on each ion were less than 0.01 eV/Å.

We have used a slab model of five atomic layers, in which the three uppermost layers were free to relax during the optimization, while the bottom two layers were kept frozen at the optimised bulk positions.

The adsorption energy per molecule was calculated from the relation

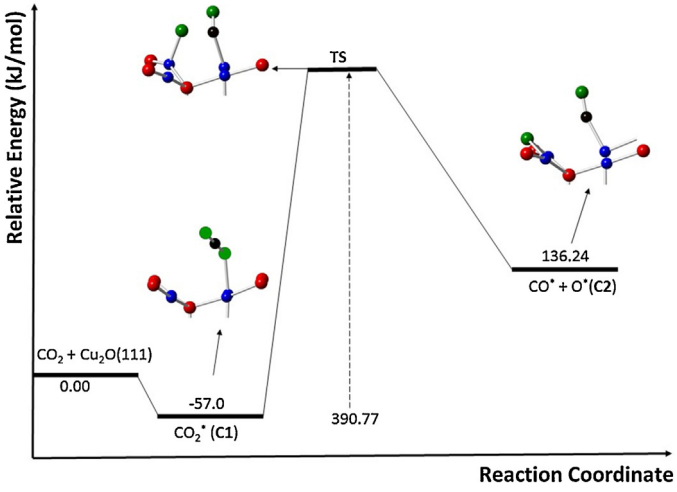

Fig. 4. Calculated potential energy diagram for the dissociation of CO_2 on the Cu_2O (111) surface. * represents an adsorbed state. Blue and red colour balls indicate Cu and O surface atoms respectively, while O and C atoms of the CO_2 molecule are represented by green and black colour balls respectively. (For interpretation of the references to colour in this figure legend, the reader is referred to the web version of this article.)

Please cite this article in press as: A.K. Mishra, N.H. de Leeuw, Mechanistic insights into the Cu(I) oxide-catalyzed conversion of CO_2 to fuels and chemicals: A DFT approach, J. CO_2 Util. (2016), http://dx.doi.org/10.1016/j.jcou.2016.02.008

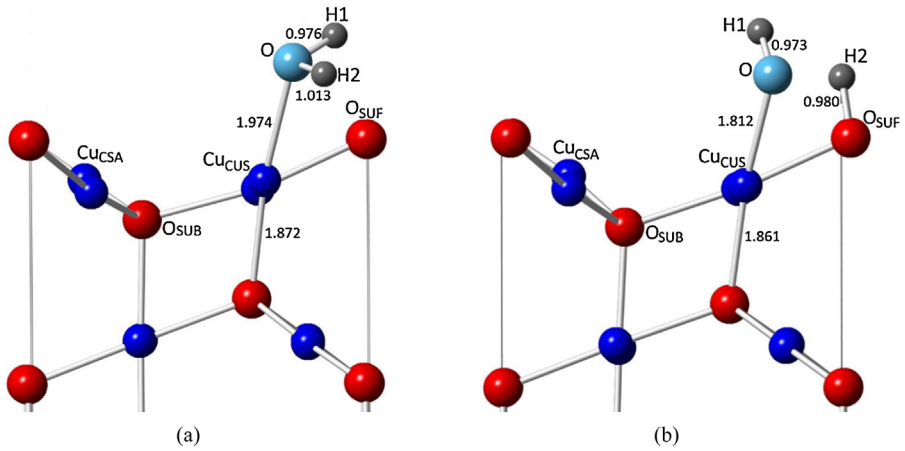

Fig. 5. The geometry of the (a) molecularly adsorbed (W–M) and (b) dissociatively adsorbed water molecule (W–D) on Cu_2O (1 1 1) surface. The bond lengths are in Å. Blue and red colour balls indicate Cu and O surface atoms respectively, while O and H atoms of H_2O are represented by light blue and grey colour balls respectively. (For interpretation of the references to colour in this figure legend, the reader is referred to the web version of this article.)

$$E_{ads} = E_{surf+mol} - (E_{surf} + E_{mol})$$

where $E_{surf+mol}$ is the total energy of the adsorbate–substrate system, E_{surf} is the energy of the naked surface slab, and E_{mol} is the energy of the isolated molecule. Within this definition, a negative adsorption energy indicates an exothermic process.

While calculating, E_{mol}, we modelled the isolated molecules in the centre of a broken symmetry cell with lattice constants of 20 Å, sampling only the Gamma-point of the Brillouin zone with the same accuracy parameters as described for the surfaces. In the case of co-adsorption and reaction on the surface, the relative energies were computed with respect to the sum of the total energies of the corresponding free molecules.

Finally, we have used the improved dimer [62,63] and climbing image nudged elastic band (CI-NEB) methods [64] to calculate the activation energy barriers and the detailed reaction coordinates for the different elementary steps.

3. Results and discussion

3.1. The Cu_2O (1 1 1) surface structure, CO_2 adsorption and dissociation

The oxygen-terminated Cu_2O (1 1 1) surface is the most stable surface among the different low-index surfaces of Cu_2O [65], consisting of four different atomic sites in the top layer, namely, a coordinatively unsaturated copper Cu_{CUS}, an outermost oxygen O_{SUF}, a coordinatively saturated copper Cu_{CSA} and a sub-surface oxygen atom O_{SUB} which is 4-fold coordinated (see Fig. 1). The (1 × 1) cell consists of two oxygen (O_{SUF}, O_{SUB}) and four copper ($3Cu_{CSA}$ and $1Cu_{CUS}$) atoms in one layer, and, as mentioned earlier, we have five layers in the slab model.

Starting from different initial orientations of the CO_2 molecule, we have investigated the adsorption of CO_2 on this surface at 1 monolayer (ML) coverage in a (1 × 1) surface cell. We found that CO_2 interacts weakly with the surface by binding to the Cu_{CUS} atom with an adsorption energy of −57.0 kJ/mol, which is in agreement with an earlier study by Bedavid et al. [66] We have also investigated CO_2 adsorption on the bigger (2 × 2) supercell (1/4 ML) where the adsorption energy increases slightly, to −61.9 kJ/mol, but with negligible changes in the adsorbed geometry.

Fig. 2 shows the adsorption geometry of CO_2 on the Cu_2O(111) surface in a (1 × 1) cell, which we chose as the initial structure (C1) to study the dissociation of CO_2 on the surface. First, we moved the O2 atom of the CO_2 molecule close to different surface sites (O_{SUB}, O_{SUF}, Cu_{CSA}), while keeping the O1 and C atoms bound to the Cu_{CUS} atom on the surface. We note that the O2 atom binds to two nearby Cu_{CSA} atoms with bond lengths of 1.868 Å and 1.869 Å, and also weakly connects to the parent Cu_{CUS} atom with a bond length of 1.955 Å. As a result of this dissociation, C-O1 binds to the surface through a C-Cu_{CUS} bond of 1.818 Å, as shown in the dissociated structure (C2) (Fig. 3).

As the dissociated O2 atom binds to the same Cu_{CUS} that is connected to C-O1 (Fig. 3a), it is worth checking the same dissociation geometry in a bigger cell to make sure that we avoid

Table 1
Adsorption energy E_{ads}, adsorbed geometry parameters and bond lengths to surface atoms for molecularly and dissociatively adsorbed water on the Cu_2O (1 1 1) surface.

	E_{ads} (kJ/mol)	∠H1—O—H2 (°)	O—H1 (Å)	O—H2 (Å)	Bond lengths to surface atoms (Å)	
					O—Cu_{CUS}	H2—O_{SUF}
W–M	−116.9	106.5	0.976	1.013	1.974	–
W–D	−101.7	–	0.973	–	1.812	0.980

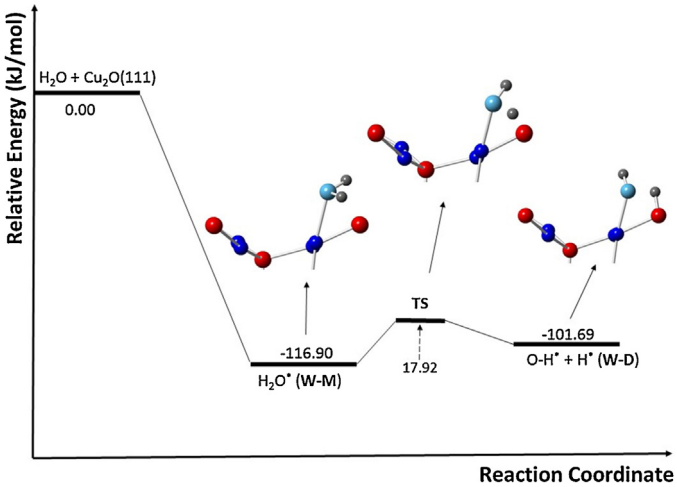

Fig. 6. Calculated potential energy diagram for the dissociation of H_2O on the Cu_2O (1 1 1) surface. * represents an adsorbed state. Blue and red colour balls indicate Cu and O surface atoms respectively, while O and H atoms of H_2O are represented by light blue and grey colour balls respectively. (For interpretation of the references to colour in this figure legend, the reader is referred to the web version of this article.)

Please cite this article in press as: A.K. Mishra, N.H. de Leeuw, Mechanistic insights into the Cu(I) oxide-catalyzed conversion of CO_2 to fuels and chemicals: A DFT approach, J. CO_2 Util. (2016), http://dx.doi.org/10.1016/j.jcou.2016.02.008

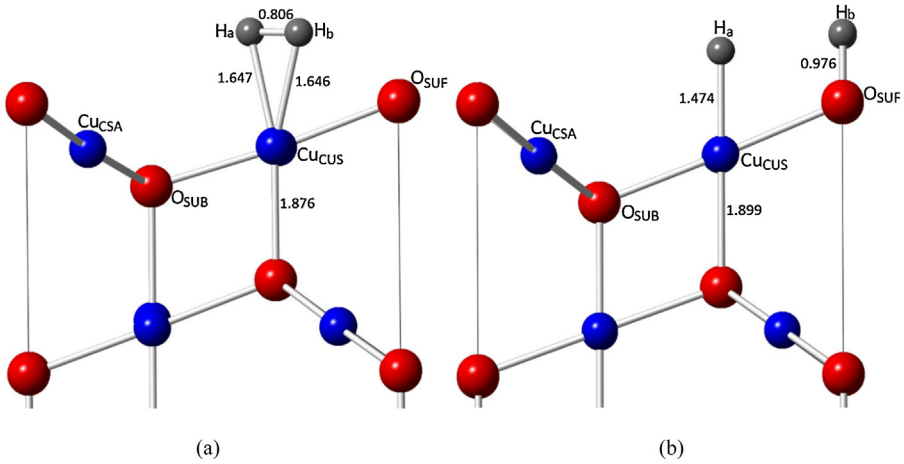

Fig. 7. The geometry of the (a) molecularly adsorbed (H–M) and (b) dissociatively adsorbed (H–D) hydrogen on Cu_2O (111) surface. The bond length values are in Å. Blue and red colour balls indicate Cu and O surface atoms respectively, while H atoms are represented by grey balls. (For interpretation of the references to colour in this figure legend, the reader is referred to the web version of this article.)

the effect of periodic images in the model, and therefore we investigated the same configuration in a bigger (2 × 1) supercell. However, calculations in the (2 × 1) supercell reveal that the CO_2 molecule dissociates in a similar fashion; here also, O2 binds to the two nearby Cu_{CSA} atoms as well as the nearby Cu_{CUS} atom. In this bigger (2 × 1) supercell, O2 binds to a different Cu_{CUS} atom from the one bonded to C-O1. As a result, it binds more strongly to Cu_{CUS}, with a 1.836 Å bond length, instead of 1.955 Å as in the (1 × 1) cell. Bond lengths with coordinatively saturated Cu_{CSA} atoms are found to be 1.902 Å and 1.903 Å. The geometries of the dissociated CO_2 molecule in both (1 × 1) and (2 × 1) supercells are shown in Fig. 3.

As we did not observe any significant changes in the dissociated geometry in the bigger (2 × 1) supercell, we investigated the CO_2 dissociation pathways in the (1 × 1) cell only to determine the activation barrier. The reaction profile (Fig. 4) indicates that formation of C1 occurs smoothly along the minimum energy path (MEP) when extending one of the C—O bonds from 1.177 to 1.188 Å and shortening the Cu_{CUS}—O surface bond to 1.885 from 1.912 Å, without a well-defined transition structure and releasing 57.0 kJ/mol. During scission of one C—O bond from the adsorbed CO_2, we found a transition state structure (TS) with a large barrier of 390.8 kJ/mol. This high barrier was expected because of the weak activation of the CO_2 molecule on the Cu_2O (111) surface.

The high value of the energy barrier to CO_2 dissociation and the overall endothermicity of the reaction indicates that the CO_2 molecule will not dissociate on the Cu_2O (111) surface under normal experimental conditions. As a next step we therefore explored the CO_2 hydrogenation pathways on the surface.

3.2. H_2O adsorption and dissociation

We first studied the molecular adsorption of water on the Cu_2O (111) surface. Here also, we explored four different surface atomic sites by placing the H_2O molecule close to these sites in different configurations. The water molecule adsorbs to the surface by binding to a Cu_{CUS} atom through its oxygen atom, at a distance of 1.974 Å (Fig. 5). We note that the adsorption of the H_2O molecule is similar to the binding of the CO_2 molecule and, as a result of the adsorption, the vertical bond distance between Cu_{CUS} (bound to the O atom of the H_2O molecule) and the topmost O atom in the second layer of the surface shortens from 1.910 to 1.872 Å. The adsorption energy calculated for the molecularly adsorbed water is −116.9 kJ/mol. In the adsorbed geometry, the O—H2 bond is stretched to 1.013 Å, compared to 0.976 Å for the O—H1 bond, with the H2 atom hydrogen-bonding to a surface O_{SUF} atom at a distance of 1.797 Å.

We also explored the dissociative adsorption of water on the Cu_2O (111) surface and found that the H2 atom binds to the surface O_{SUF} atom at 0.980 Å. The hydroxyl (O—H1) interacts with the Cu_{CUS} more strongly at 1.812 Å. The adsorption energy in this configuration is −101.7 kJ/mol, indicating that molecular adsorption is favoured over dissociative adsorption on the Cu_2O (111) surface. The adsorbed geometries and adsorption energies for both molecular and dissociative adsorption are summarized in Table 1. We further calculated the transition state for water dissociation on the surface and found that the water molecule could dissociate easily with a very low energy barrier of 17.9 kJ/mol. The geometry of the transition state structure along with potential energy diagram for water dissociation is shown in Fig. 6.

3.3. H_2 adsorption and dissociation

Similar to the water adsorption, we have examined the adsorption of hydrogen on the Cu_2O (111) surface, both

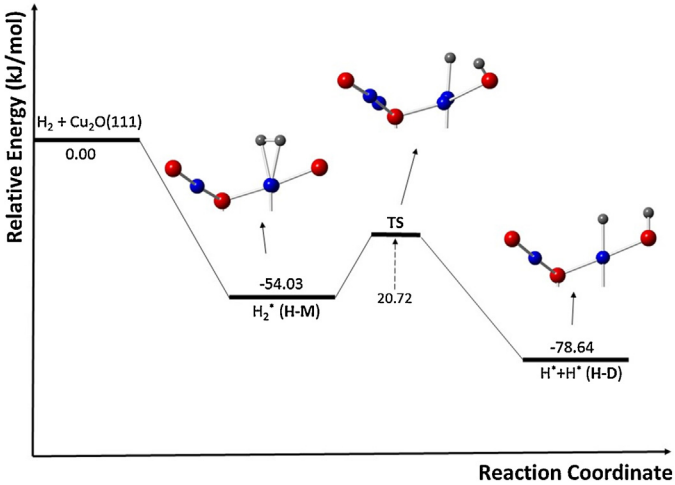

Fig. 8. Calculated potential energy diagram for the dissociation of H_2 on the Cu_2O (111) surface. * represents an adsorbed state. Blue and red colour balls indicate Cu and O surface atoms respectively, while H atoms are represented by grey balls. (For interpretation of the references to colour in this figure legend, the reader is referred to the web version of this article.)

Please cite this article in press as: A.K. Mishra, N.H. de Leeuw, Mechanistic insights into the Cu(I) oxide-catalyzed conversion of CO_2 to fuels and chemicals: A DFT approach, J. CO_2 Util. (2016), http://dx.doi.org/10.1016/j.jcou.2016.02.008

Table 2
The adsorption energies E_{ads}, adsorbed geometry parameters and bond lengths to surface atoms for molecularly and dissociatively adsorbed hydrogen on the Cu_2O (111) surface.

	E_{ads} (kJ/mol)	H_a—H_b (Å)	Bond lengths to surface atoms (Å)		
			H_a—Cu_{CUS}	H_b—Cu_{CUS}	H_b—O_{SUF}
H–M	−54.0	0.806	1.647	1.646	–
H–D	−78.6	–	1.474	–	0.976

molecularly and dissociatively. We have tried different initial configurations, by placing the H_2 molecule in parallel and perpendicular directions with respect to the top surface layer and exploring different possible surface sites. The H_2 molecule binds to the surface through a Cu_{CUS} atom, with Cu_{CUS}—H_a and Cu_{CUS}—H_b bond lengths of 1.647 Å and 1.646 Å respectively [Fig. 7]. The H_a—H_b bond length becomes slightly elongated to 0.806 Å. In all the configurations where we placed the H_2 molecule close to the O_{SUB} and O_{SUF} atom, the molecule moves away from the surface without binding to it, but in the configurations close to the coordinatively saturated Cu_{CSA} atoms, the molecule binds to the Cu_{CUS} atom. The adsorption energy for the molecularly adsorbed hydrogen (H–M) molecule is −54.0 kJ/mol.

We next studied the dissociative adsorption and found that one of the hydrogen atoms (H_b) binds to the topmost O_{SUF} atom, similar to the H_2O dissociation, leaving the other atom (H_a) bound to the coordinatively unsaturated, $Cu_{CUS,}$ atom. The adsorption energy in this case (H–D) is −78.6 kJ/mol, i.e. energetically more favourable than the molecular adsorption. The bond length of the surface Cu_{CUS} atom to the oxygen atom in the second layer is found to be ~1.90 Å, which is slightly larger than that in molecular adsorption (1.876 Å). The geometries of molecularly adsorbed (H–M) and dissociatively adsorbed (H–D) hydrogen along with relevant interatomic distances are presented in Fig. 7. We note that after dissociation, the H_b atom binds strongly to the surface oxygen O_{SUF}, with a bond length of 0.976 Å, while the H_a—Cu_{CUS} bond length is found to be 1.474 Å. In order to further analyse the nature of the bonding, we have calculated the Bader charges of the hydrogen atoms, H_a, H_b, and the surface atoms, Cu_{CUS}, O_{SUF}, to which they are bound. We note that H_b transfers charge to the surface O_{SUF} atom, becoming H_b^+ with a 0.67 positive charge, while H_a accepts electrons from Cu_{CUS} to become H_a^- with −0.29 charge. As such, the hydrogen molecule has dissociated into a proton and hydride species, where one hydrogen atom transfers charge to a comparatively more electronegative surface oxygen atom, while the other hydrogen atom gains charge from a comparatively less electronegative surface copper atom.

We next examined the energy barrier for the H_2 dissociation and found that a low energy of 20.7 kJ/mol is required to dissociate the molecularly adsorbed H_2 on the Cu_2O (111) surface. The geometry of the transition state together with relative energy values are given in Fig. 8. Table 2 summarizes the adsorption energies and geometrical parameters for both molecularly and dissociatively adsorbed hydrogen.

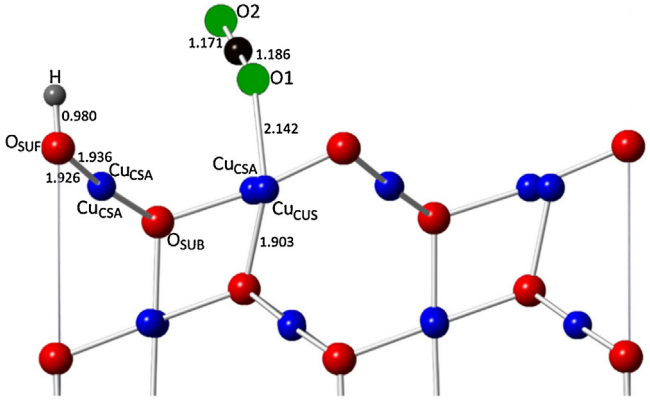

(a)

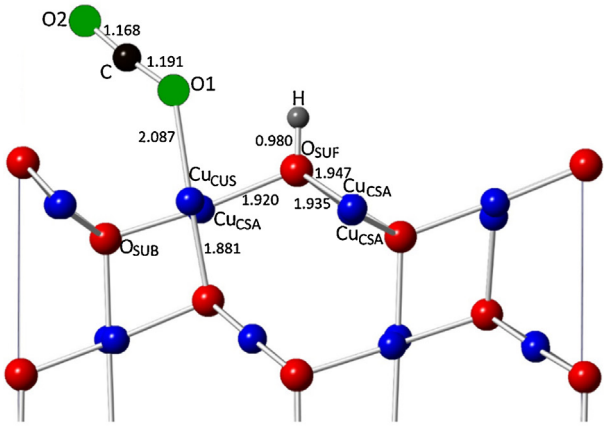

(b)

Fig. 9. Two configurations of co-adsorption of CO_2 molecule and the H adatom on Cu_2O (111) surface in (2 × 1) supercell, CH1 (a) and CH2 (b). Blue and red colour balls indicate Cu and O surface atoms respectively, while O and C atoms of the CO_2 molecule are represented by green and black colour balls respectively and hydrogen atom is represented by a grey colour ball. (For interpretation of the references to colour in this figure legend, the reader is referred to the web version of this article.)

Please cite this article in press as: A.K. Mishra, N.H. de Leeuw, Mechanistic insights into the Cu(I) oxide-catalyzed conversion of CO_2 to fuels and chemicals: A DFT approach, J. CO_2 Util. (2016), http://dx.doi.org/10.1016/j.jcou.2016.02.008

The results of CO_2, H_2O and H_2 adsorption on the perfect Cu_2O (111) surface show that Cu_{CUS} is the most reactive site on the surface, while the topmost surface oxygen atom, O_{SUF}, shows affinity towards atomic hydrogens. The transition state calculations show that the barriers to the dissociation of H_2O and H_2 on the (111) surface are very small, suggesting routes towards a source of hydrogen for the hydrogenation of CO_2. In the next section we discuss the co-adsorption and hydrogenation of the CO_2 molecule on the Cu_2O (111) surface.

3.4. Co-adsorption of CO_2 and H adatom

We first examined the co-adsorption of the CO_2 molecule and the H adatom in a (1×1) supercell. We started from the CO_2 molecule adsorbed on the surface and investigated the co-adsorption of the H adatom on different sites. However, in all the configurations tried, the CO_2 molecule starts moving away from the surface, with the most stable configuration one in which the H adatom binds to the topmost surface oxygen O_{SUF}, but with the CO_2 molecule desorbed from the surface. We noted that the distance between the periodic images of the CO_2 molecule is about 4 Å in the *x*-direction, while in the *y*-direction it is more than 6 Å. Hence, we re-examined all the configurations in a (2×1) supercell (doubled in the *x*-direction) to avoid the effect of periodic images.

In a (2×1) super cell, we noted that the CO_2 molecule remains bound to the Cu_{CUS} atom, with the H adatom binding to the O_{SUF} atom on the surface. In this supercell, we have two O_{SUF} atomic sites and both show equal affinity for the H adatom and accordingly we obtain two configurations, CH1 (Fig. 9a) and CH2 (Fig. 9b), for the co-adsorption of CO_2 and the H adatom. We note that configuration CH2 is less stable than CH1 by just 2.1 kJ/mol, suggesting the co-existence of both configurations.

The addition of an H adatom near the pre-adsorbed CO_2, weakens the binding of the CO_2 molecule to the surface, as the O1—Cu_{CUS} bond distance increases from 2.046 to 2.142 and 2.087 Å for the CH1 and CH2 configurations, respectively. Also, in order to bind to the H adatom, the surface O_{SUF} atom moves up, increasing its bond lengths to three neighbouring Cu_{CSA} atoms to 1.926, 1936 and 1.944 Å, from about 1.823 Å in CH1, while it increases to 1.947, 1.935 and 1.920 Å, respectively, for three Cu_{CSA} atoms in CH2.

We calculated the adsorption energies with reference to the free CO_2 and H_2 molecules using the following relation:

$$E_{ads}(CH) = E_{Cu_{2O(CO_2+H)}} - \left[E_{Cu_{2O}} + E_{CO_2} + 1/2E_{H_2}\right]$$

where E_{CO_2+H} is the energy of the co-adsorbed CO_2 molecule and H adatom, E_{Cu_2O} is the energy of the Cu_2O surface, E_{CO_2} is the energy of the free CO_2 molecule and E_{H_2} is the energy of the free H_2 molecule.

The adsorption energies for the CH1 and CH2 configurations are found to be −48.9 and −51.1 kJ/mol respectively, indicating

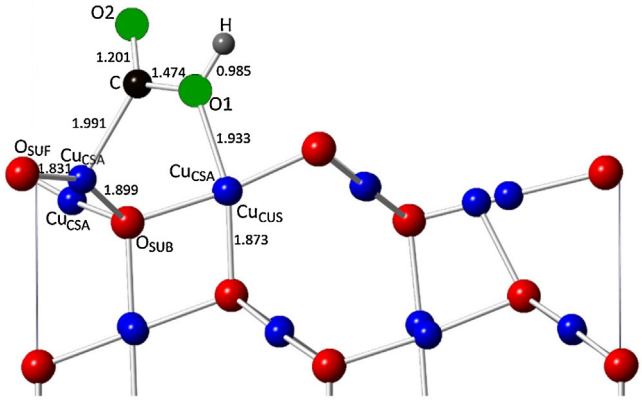

(a)

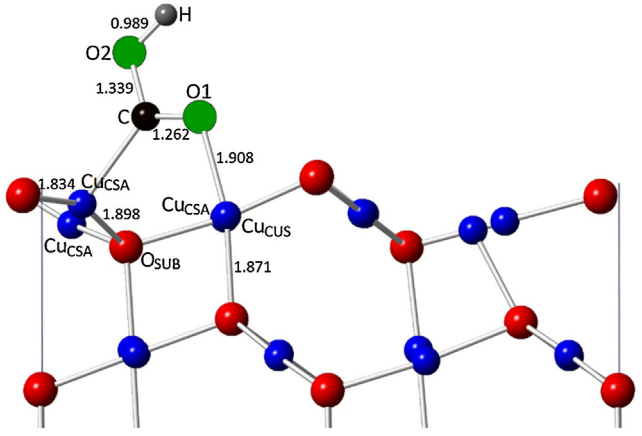

(b)

Fig. 10. Two possible configurations, (a) CB1 and (b) CB2 (b) for carboxyl formation on the Cu_2O (111) surface. Blue and red colour balls indicate Cu and O surface atoms respectively, while O, C and H atoms of the molecule are represented by green, black and grey colour balls respectively. (For interpretation of the references to colour in this figure legend, the reader is referred to the web version of this article.)

Please cite this article in press as: A.K. Mishra, N.H. de Leeuw, Mechanistic insights into the Cu(I) oxide-catalyzed conversion of CO_2 to fuels and chemicals: A DFT approach, J. CO_2 Util. (2016), http://dx.doi.org/10.1016/j.jcou.2016.02.008

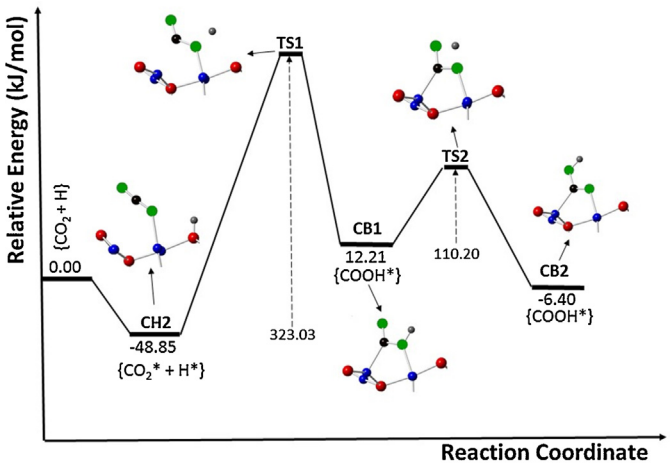

Fig. 11. Calculated possible potential energy diagram for the carboxyl formation on the Cu_2O (111) surface.* represents an adsorbed state. Blue and red colour balls indicate Cu and O surface atoms respectively, while O, C and H atoms of the molecule are represented by green, black and grey colour balls respectively. (For interpretation of the references to colour in this figure legend, the reader is referred to the web version of this article.)

exothermic reactions, although the co-adsorption energies are smaller than the adsorption of CO_2 and H_2 molecules separately, reflecting weaker binding.

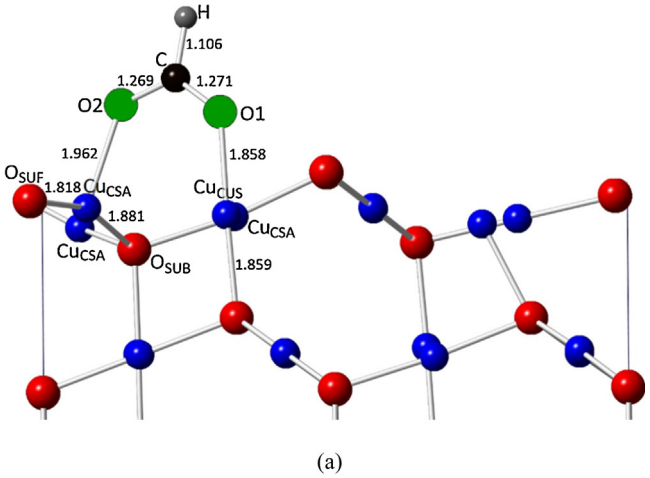

(a)

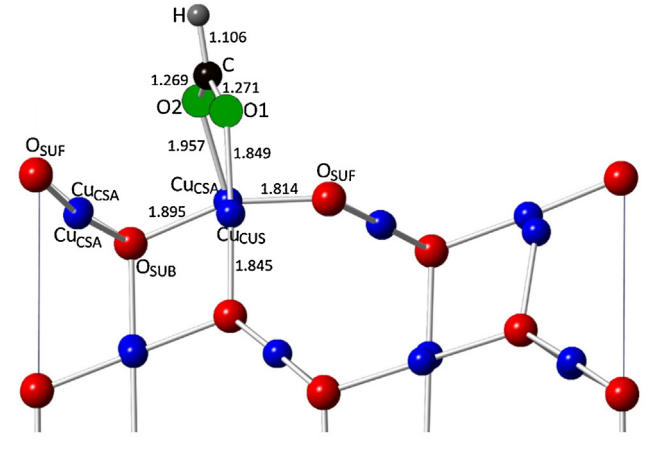

(b)

Fig. 12. Two possible configurations, **FM1** (a) and **FM2** (b) for formate formation on Cu_2O (111) surface. Blue and red colour balls indicate Cu and O surface atoms respectively, while O, C and H atoms of the molecule are represented by green, black and grey colour balls respectively. (For interpretation of the references to colour in this figure legend, the reader is referred to the web version of this article.)

3.5. CO_2 hydrogenation to carboxyl and formate intermediates

Having identified the most favourable co-adsorption structure for CO_2 and the H adatom, our next goal is to identify the nature of the intermediates formed in the carboxyl and formate reaction mechanism, as the H adatom can attack the adsorbed CO_2 molecule to form either carboxyl (CB) or formate (FM) species. We first investigated the detailed reaction coordinate of CO_2 hydrogenation to the carboxyl intermediate (COOH), a key intermediate for the low-temperature water–gas shift (WGS) reaction [67–69]. For carboxyl formation, the H adatom can attack either the O1 or O2 atom of the adsorbed CO_2 on the Cu_2O surface and accordingly we have two carboxyl configurations, CB1 and CB2 respectively (Fig. 10). We note that during carboxyl formation, the surface Cu_{CSA} atom moves up to bind to the C atom of the CO_2 molecule, increasing the bond lengths to surface O_{SUB} and O_{SUF} atoms to 1.899 and 1.831 Å in CB1 and to 1.898 and 1.834 Å in CB2 from their original values of 1.863 and 1.823 Å, respectively.

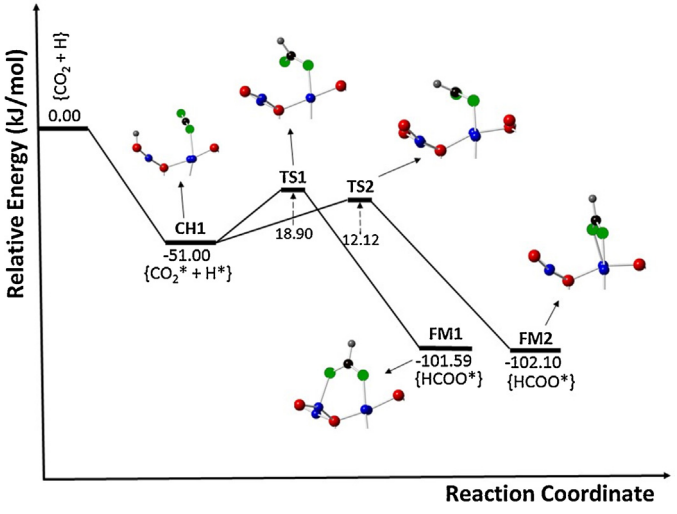

Fig. 13. Calculated potential energy diagram for the formate formation on the Cu_2O (111) surface.* represents an adsorbed state. Blue and red colour balls indicate Cu and O surface atoms respectively, while O, C and H atoms of the molecule are represented by green, black and grey colour balls respectively. (For interpretation of the references to colour in this figure legend, the reader is referred to the web version of this article.)

Please cite this article in press as: A.K. Mishra, N.H. de Leeuw, Mechanistic insights into the Cu(I) oxide-catalyzed conversion of CO_2 to fuels and chemicals: A DFT approach, J. CO_2 Util. (2016), http://dx.doi.org/10.1016/j.jcou.2016.02.008

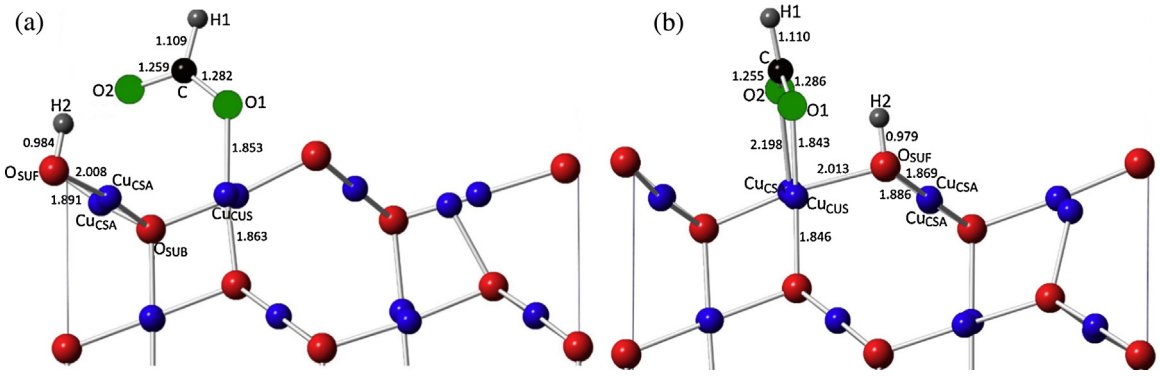

Fig. 14. The two configurations, (a) **FMH1** and (b) **FMH2** of the co-adsorption of formate and atomic hydrogen on the Cu_2O (111) surface. All the bond lengths are in Å. Blue and red colour ball indicates Cu and O surface atoms respectively, while O, C and H atoms of the molecule are represented by green, black and grey colour balls respectively. (For interpretation of the references to colour in this figure legend, the reader is referred to the web version of this article.)

The two carboxyl intermediates (CB1 and CB2) differ in energy by only ~18.6 kJ/mol, with CB2 being the more stable. We first investigated the transition state and barrier for carboxyl formation by choosing CH2 as the CO_2 and H adatom co-adsorption configuration. We found that the H adatom adsorbed on the surface first binds to the O1 atom to form CB1, but with a very high barrier of ~323 kJ/mol. To obtain the more stable CB2 configuration, a second transition state, TS2, is identified with a barrier of ~110 kJ/mol, as shown in Fig. 11. Hence, our transition state calculations show that large energy barriers need to be overcome for the formation of carboxyl on the Cu_2O (111) surface.

We subsequently studied an alternative route for the hydrogenation of CO_2 to formic acid through the formate intermediate (HCOO). The binding of the H adatom with the carbon atom results in formate (FM1) formation, where we note that the CO_2 molecule bends and one of the surface Cu_{CSA} atoms moves up to bind to the O2 atom of the CO_2 molecule, changing the bond distance from O_{SUF} and O_{SUB} atoms from 1.824 and 1.863 Å to 1.818 and 1.881 Å, respectively (Fig. 12a).

Another similar configuration, FM2, is shown in Fig. 12b, where the O2 atom binds to a different Cu_{CSA} atom, but in a similar fashion as in FM1. This configuration is negligibly more stable compared to FM1 (by ~0.5 kJ/mol). We found that formate is more stable than the carboxyl intermediate by about ~96 kJ/mol and we therefore investigated the formate formation route on the Cu_2O (111) surface by determining transition states and activation barriers for both FM1 and FM2. The transition state calculations show that a small barrier of 12.1 kJ/mol is required to form configuration FM2, while a barrier of 18.9 kJ/mol is needed to form FM1. The CO_2 molecule bends and the H atom moves towards the carbon atom to form the transition state structures shown in Fig. 13.

As formate is more stable than the carboxyl intermediate and as very small activation barriers are needed to form formate moieties at the surface, compared to the very high activation barrier values for the formation of carboxyl, we have next studied the second hydrogenation reaction, from the formate intermediate to formic acid.

3.6. Formic acid formation

We first studied the co-adsorption of a second hydrogen and the formate on the surface. As mentioned before, in a (2 × 1) supercell slab we have two similar O_{SUF} atomic sites where a second hydrogen atom can bind to the surface. We note that irrespective of whether we choose FM1 or FM2, placing the second hydrogen gives two similar configurations, FMH1 and FMH2, as shown in Fig. 14. In both configurations, we observe that the formate tends to become oriented towards the hydrogen (H2) adsorbed at the O_{SUF} surface atom, with FMH2 being more stable by 5.8 kJ/mol.

We further investigated the lowest energy configurations of formic acid on the surface by attaching the second hydrogen, H2, to the formate geometry (FM2). In all configurations tried, we found that the H2 atom binds to both O2 and a surface oxygen, O_{SUF}. The

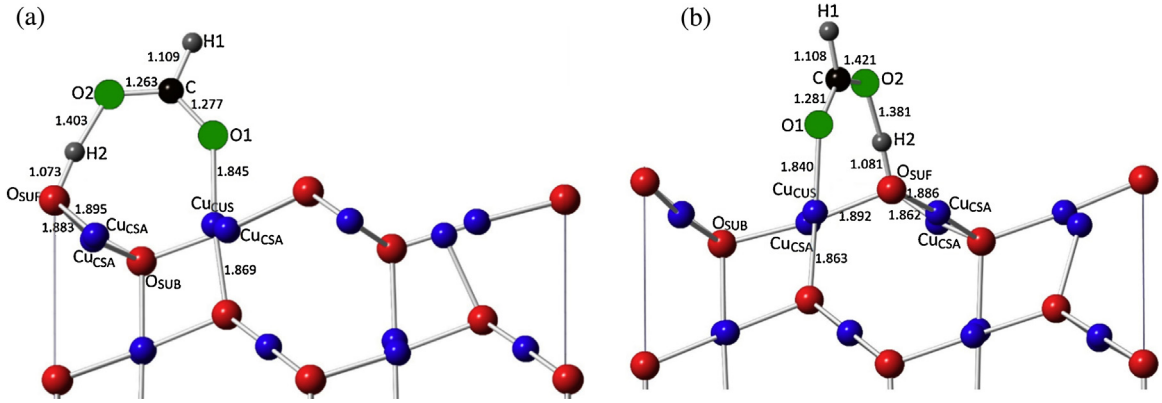

Fig. 15. The two configurations, (a) **FR1** and (b) **FR2** of the formic acid formation on the Cu_2O (111) surface. All the bond lengths are in Å. Blue and red colour ball indicates Cu and O surface atoms respectively, while O, C and H atoms of the molecule are represented by green, black and grey colour balls respectively. (For interpretation of the references to colour in this figure legend, the reader is referred to the web version of this article.)

Please cite this article in press as: A.K. Mishra, N.H. de Leeuw, Mechanistic insights into the Cu(I) oxide-catalyzed conversion of CO_2 to fuels and chemicals: A DFT approach, J. CO_2 Util. (2016), http://dx.doi.org/10.1016/j.jcou.2016.02.008

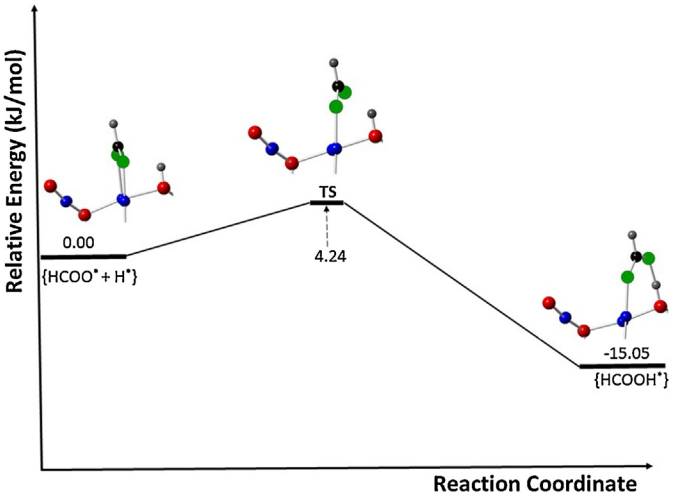

Fig. 16. Calculated potential energy diagram for formic acid formation on Cu_2O (111) surface.* represents the adsorbed state. Blue and red colour balls indicate Cu and O surface atoms respectively, while O, C and H atoms of the molecule are represented by green, black and grey colour balls respectively. (For interpretation of the references to colour in this figure legend, the reader is referred to the web version of this article.)

O2—H2 and H2—O_{SUF} bond lengths are found to be 1.403 and 1.073 Å, respectively, in the first configuration, FR1, while in a second configuration, FR2, which is more stable by ~8.1 kJ/mol, O2—H2 and H2—O_{SUF} bond lengths are 1.381 and 1.081 Å, respectively, reflecting a strong interaction of the compound with the surface through O_{SUF}-H2 bonding (Fig. 15).

As a next step, we performed transition state calculations to determine the activation energy barrier from FMH2 to the most stable formic acid configuration FR2. We found that a very small activation energy of only 4.2 kJ/mol is required for the formic acid formation. The transition state structure together with relative energies and activation barrier is shown in Fig. 16. From the transition state structure, we observe that during formic acid formation, the weak O2—Cu_{CSA} bond (2.198 Å) with the surface is broken and O2 becomes oriented towards the adsorbed H-atom. The H2 atom also inclines towards the O2 atom with an increase in the O_{SUF}—H2 bond length from 0.979 to 1.009 Å.

The calculated adsorption energy for formic acid is −198.9 kJ/mol on the Cu_2O (111) surface, which is much larger than for H_2O (−116.9 kJ/mol) and CO_2 (−57.0 kJ/mol), thus binding more strongly to the surface, which may make release from the surface difficult.

4. Conclusions

We have presented a theoretical study, using dispersion corrected DFT + U, to investigate CO_2 conversion on the Cu_2O (111) surface. Our calculations show that a very large activation barrier is required to dissociate the physisorbed CO_2 molecule on the Cu_2O (111) surface. The water molecule shows strong binding to the surface, with molecular adsorption preferred, whereas hydrogen is more likely to adsorb dissociatively, although less strongly. The activation barrier for dissociation of both H_2O and H_2 is found to be very low (≤20 kJ/mol), suggesting possible sources of hydrogen for CO_2 hydrogenation. We next investigated CO_2 hydrogenation and determined the reaction kinetics by exploring the formation of two possible intermediate, viz, carboxyl and formate, towards formic acid formation. The calculations show that carboxyl formation is not energetically favourable with very large activation barriers, while the formation of formate is an exothermic reaction with a low value (~12 kJ/mol) for the activation energy barrier. Calculation of the second hydrogenation to form formic acid from formate reveals that formic acid forms very rapidly with an activation energy of just ~4 kJ/mol, although the formic acid product is strongly bound to the surface. Our work suggests that Cu_2O may be a suitable catalyst for CO_2 conversion to formate and formic acid under mild conditions.

Acknowledgements

This work was carried out as part of the Engineering and Physical Sciences Research Council (EPSRC) “4CU” programme grant, aimed at sustainable conversion of carbon dioxide into fuels, led by The University of Sheffield and in collaboration with University College London, the University of Manchester and Queen’s University Belfast. The authors acknowledge the EPSRC for supporting this work financially (Grant Nos. EP/K001329/1 and EP/K035355/1). ‘Via our membership of the UK’s HEC Materials Chemistry Consortium, which is funded by EPSRC (EP/L000202), this work used the ARCHER UK National Supercomputing Service (http://www.archer.ac.uk). The authors also acknowledge the use of the IRIDIS High Performance Computing Facility, and associated support services at the University of Southampton, in the completion of this work. NHdL thanks the Royal Society for an Industry Fellowship.

References

[1] R. Nataly Echevarria Huaman, T. Xiu Jun, Renewable Sustainable Energy Rev. 31 (2014) 368–385.
[2] Z. Jiang, T. Xiao, V.L. Kuznetsov, P.P. Edwards, Philos. Trans. A Math. Phys. Eng. Sci. 2010 (1923) 3343–3364.
[3] Pieter Tans, NOAA/ESRL (www.esrl.noaa.gov/gmd/ccgg/trends/) and Ralph Keeling, Scripps Institution of Oceanography (scrippsco2.ucsd.edu/).
[4] Ed Dlugokencky and Pieter Tans, NOAA/ESRL (www.esrl.noaa.gov/gmd/ccgg/trends/).
[5] IPCC, Climate Change 2007—The Physical Science Basis. Contribution of Working Group I to the Fourth Assessment Report of the Intergovernmental Panel on Climate Change, Cambridge University Press, 2007, pp. 996.
[6] K.Z. House, A.C. Baclig, M. Ranjan, E.A. van Nierop, J. Wilcox, H.J. Herzog, Proc. Natl. Acad. Sci. 108 (2011) 20428–20433.
[7] M. Aresta, A. Dibenedetto, Dalton Trans. 2007 (2016) 2975–2992.
[8] L.N. He, J.Q. Wang, J.L. Wang, Pure Appl. Chem. 81 (2009) 2069–2080.
[9] O. Jacquet, X. Frogneux, C. Das Neves Gomes, T. Cantat, Chem. Sci. 4 (2013) 2127–2131.
[10] Z. Han, L. Rong, J. Wu, L. Zhang, Z. Wang, K. Ding, Angew. Chem. Int. Ed. 51 (2012) 13041–13045.

Please cite this article in press as: A.K. Mishra, N.H. de Leeuw, Mechanistic insights into the Cu(I) oxide-catalyzed conversion of CO_2 to fuels and chemicals: A DFT approach, J. CO_2 Util. (2016), http://dx.doi.org/10.1016/j.jcou.2016.02.008

[11] Z.Z. Yang, L.N. He, J. Gao, A.H. Liu, B. Yu, Energy Environ. Sci. 5 (2012) 6602–6639.
[12] M. Aresta, A. Dibenedetto, A. Angelini, Chem. Rev. 114 (2014) 1709–1742.
[13] Q. Liu, L. Wu, R. Jackstell, M. Beller, Nat. Commun. 6 (2015) 5933.
[14] P. Kaiser, R.B. Unde, C. Kern, A. Jess, Chemie-Ingenieur-Technik 85 (2013) 489–499.
[15] H.C. Butterman, M.J. Castaldi, Environ. Sci. Technol. 43 (2009) 9030–9037.
[16] M.G. Mura, L. De Luca, G. Giacomelli, A. Porcheddu, Adv. Synth. Catal. 354 (2012) 3180–3186.
[17] W. Leitner, Angew. Chem. Int. Ed. (English) 34 (1995) 2207–2221.
[18] S. Moret, P.J. Dyson, G. Laurenczy, Nat. Commun. 5 (2014) 4017.
[19] B. Loges, A. Boddien, H. Junge, M. Beller, Angew. Chem. Int. Ed. 47 (2008) 3962–3965.
[20] F. Joó, ChemSusChem 1 (2008) 805–808.
[21] S. Enthaler, J. Von Langermann, T. Schmidt, Energy Environ. Sci. 3 (2010) 1207–1217.
[22] B. Loges, A. Boddien, F. Gärtner, H. Junge, M. Beller, Top. Catal. 53 (2010) 902–914.
[23] M. Aresta, A. Dibenedetto, J. Braz. Chem. Soc. 25 (2016) 2215–2228.
[24] G. Centi, E.A. Quadrelli, S. Perathoner, Energy Environ. Sci. 6 (2013) 1711–1731.
[25] P.G. Jessop, R.H. Morris, Coord. Chem. Rev. 121 (1992) 155–284.
[26] P.G. Jessop, T. Ikariya, R. Noyori, Chem. Rev. 95 (1995) 259–272.
[27] O. Krocher, R.A. Koppel, A. Baiker, Chem. Commun. 1997 (2016) 453–454.
[28] S. Sakaki, Y. Musashi, J. Am. Chem. Soc 122 (2010) 3867–3877.
[29] A. Roldan, N. Hollingsworth, A. Roffey, H.-U. Islam, J.B.M. Goodall, C.R.A. Catlow, J.A. Darr, W. Bras, G. Sankar, K.B. Holt, G. Hogarth, N.H. de Leeuw, Chem. Commun. 51 (2015) 7501–7504.
[30] A.F.A.-P. Andrew Peterson, Felix Studt, Jan Rossmeisl, K. Jens Nørskov, Energy Environ. Sci. 3 (2010) 1311–1315.
[31] X. Liang, L. Gao, S. Yang, Sun J. Adv. Mater. 2 (2009) 2068–2071.
[32] J. Liu, J. Jin, Z. Deng, S.Z. Huang, Z.Y. Hu, L. Wang, C. Wang, L.H. Chen, Y. Li, G.V. Tendeloo, B.L. Su, J. Colloid Interface Sci. 384 (2012) 1–9.
[33] X. Zhang, W. Shi, J. Zhu, D.J. Kharistal, W. Zhao, B.S. Lalia, H.H. Hng, Q. Yan, ACS Nano 5 (2011) 2013–2019.
[34] L.B. Chen, N. Lu, C.M. Xu, H.C. Yu, T.H. Wang, Electrochim. Acta 54 (2009) 4198–4201.
[35] A. Aslani, V. Oroojpour, Phys. B Condens. Matter 406 (2011) 144–149.
[36] I. Ali, Chem. Rev. 112 (2012) 5073–5091.
[37] S.B. Wang, C.H. Hsiao, S.J. Chang, K.T. Lam, K.H. Wen, S.C. Hung, S.J. Young, B.R. Huang, Sen. Actuators A Phys. 171 (2011) 207–211.
[38] X. Liang, L. Gao, S. Yang, Sun J. Adv. Mater. 2 (2009) 2068–2071.
[39] K. Rajeshwar, N.R. Tacconi de, G. Ghadimkhani, W. Chanmanee, C. Janáky, Chemphyschem 14 (2013) 2251–2259.
[40] M. Le, M. Ren, Z. Zhang, P.T. Sprunger, R.L. Kurtz, J.C. Flake, J. Electrochem. Soc. 158 (2011) E45–E49.
[41] O. Lupan, V. Cretu, V. Postica, N. Ababii, O. Polonskyi, V. Kaidas, F. Schütt, Y.K. Mishra, E. Monaico, I. Tiginyanu, et al., Sens. Actuators B Chem. 224 (2016) 434–448.
[42] J.K. Nørskov, T. Bligaard, J. Rossmeisl, C.H. Christensen, Nat. Chem. 1 (2009) 37–46.
[43] M. Le, M. Ren, Z. Zhang, P.T. Sprunger, R.L. Kurtz, J.C. Flake, J. Electrochem. Soc. 158 (2011) E45.
[44] B. Morreale, F. Shi, Novel Materials for Carbon Dioxide Mitigation Technology. Novel Materials for Carbon Dioxide Mitigation Technology, 04 Jun 2015, pp. 414.
[45] J. Ye, C. Liu, Q. Ge, J. Phys. Chem. C 116 (2012) 7817–7825.
[46] R.J. Lim, M. Xie, M.A. Sk, J.-M. Lee, A. Fisher, X. Wang, K.H. Lim, Catal. Today 233 (2014) 169–180.
[47] D. Cheng, F.R. Negreiros, E. Aprà, A. Fortunelli, ChemSusChem 6 (2013) 944–965.
[48] Y. Yang, J. Evans, J.A. Rodriguez, M.G. White, P. Liu, Phys. Chem. Chem. Phys. 12 (2010) 9909–9917.
[49] Q.L. Tang, Q.J. Hong, Z.P. Liu, J. Catal. 263 (2009) 114–122.
[50] G. Kresse, J. Furthmüller, Comput. Mater. Sci. 6 (1996) 15–50.
[51] G. Kresse, J. Furthmüller, Phys. Rev. B 54 (1996) 11169–11186.
[52] G. Kresse, J. Hafner, Phys. Rev. B 49 (1994) 14251–14269.
[53] G. Kresse, J. Hafner, Phys. Rev. B 47 (1993) 558–561.
[54] P.E. Blöchl, Phys. Rev. B 50 (1994) 17953–17979.
[55] J.P. Perdew, K. Burke, M. Ernzerhof, Phys. Rev. Lett. 78 (1997) 1396.
[56] J.P. Perdew, K. Burke, M. Ernzerhof, Phys. Rev. Lett. 77 (1996) 3865–3868.
[57] S.L. Dudarev, G.A. Botton, S.Y. Savrasov, C.J. Humphreys, A.P. Sutton, Phys. Rev. B 57 (1998) 1505–1509.
[58] A.K. Mishra, A. Roldan, N.H.d.l. Leeuw, J. Phys. Chem. C 120 (2016) 2198–2214.
[59] S. Grimme, J. Comput. Chem. 27 (2006) 1787–1799.
[60] H.J. Monkhorst, J.D. Pack, Phys. Rev. B 13 (1976) 5188–5192.
[61] P.E. Blöchl, O. Jepsen, O.K. Andersen, Phys. Rev. B 49 (1994) 16223–16233.
[62] G. Henkelman, H. Jónsson, J. Chem. Phys. 111 (1999) 7010–7022.
[63] A. Heyden, A.T. Bell, F.J. Keil, J. Chem. Phys. 123 (2005) 224101–224115.
[64] G. Henkelman, B.P. Uberuaga, H. Jónsson, J. Chem. Phys. 113 (2000) 9901–9904.
[65] A. Soon, M. Todorova, B. Delley, C. Stampfl, Phys. Rev. B 75 (2007) 125420–125428.
[66] L.I. Bendavid, E.A. Carter, J. Phys. Chem. C 117 (2013) 26048–26059.
[67] Y. Yang, C.A. Mims, D.H. Mei, C.H.F. Peden, C.T. Campbell, J. Catal. 298 (2013) 10–17.
[68] R.C. Catapan, A.A.M. Oliveira, Y. Chen, D.G. Vlachos, J. Phys. Chem. C 116 (2012) 20281–20291.
[69] J.A. Herron, J. Scaranto, P. Ferrin, S. Li, M. Mavrikakis, ACS Catal. 4 (2014) 4434–4445.

Please cite this article in press as: A.K. Mishra, N.H. de Leeuw, Mechanistic insights into the Cu(I) oxide-catalyzed conversion of CO_2 to fuels and chemicals: A DFT approach, J. CO_2 Util. (2016), http://dx.doi.org/10.1016/j.jcou.2016.02.008